PROCEEDINGS OF SCIENCE

Top-quark effects in diphoton production through gluon fusion at NLO in QCD

Xiaoran Zhao*
Centre for Cosmology, Particle Physics and Phenomenology (CP3), Université catholique de Louvain, Belgium
E-mail: xiaoran.zhao@uclouvain.be

Diphoton production is one important channel at hadron colliders. Gluon fusion into diphoton via quark loops provide a substantial contribution. When the top quark mediated contribution is negligible below the top pair threshold, it becomes important at the threshold and above. We present the first complete computation of the next-to-leading order(NLO) corrections to this process, including contributions from the top quark. The analytical expression for relevant two-loop diagrams are unknown and we developed a numerical algorithm to compute them. We found that NLO corrections is large over all kinematic regions. The top quark contribution leads to change of slope below and above the top pair threshold, and it is more visible at NLO. We further find that above the top quark threshold, NLO corrections is larger after including the top quark contribution.

14th International Symposium on Radiative Corrections (RADCOR2019)
9-13 September 2019
Palais des Papes, Avignon, France

*Speaker.

© Copyright owned by the author(s) under the terms of the Creative Commons Attribution-NonCommercial-NoDerivatives 4.0 International License (CC BY-NC-ND 4.0).

PoS(RADCOR2019)024

1. Introduction

The production of a pair of photons (diphoton) is an important process at hadron colliders. The final state signature is experimentally clean, and experimental measurements are available at Tevatron[1, 2] and LHC[3, 4]. It is one golden channel for the discovery of the Higgs boson[5, 6], and $H \to \gamma\gamma$ remains one of the cleanest final states to study the properties of the Higgs boson. Diphoton channel is also very important channel on searching new physics beyond the Standard Model[7, 8], including new scalar or spin-2 reasonance, multiple resonances from extra-dimension/clockwork models[9, 10, 11, 12], or peak-dip structures due to new particles in loops[13].

At leading order, it is produced through quark-antiquark annihilation. Next-to-Leading order(NLO) corrections to this process has been known since 2000[14]. Recently, NNLO corrections are also know and available in public code[15, 16, 17]. In addition to quark-antiquark annihilation, diphoton can also be produced through gluon fusion. Formally it can be counted as part of NNLO corrections to $q\bar{q} \to \gamma\gamma$. However, due to large gluon-gluon luminosity, the contribution from gluon fusion is anomalous large. Since the gluon fusion process is separately gauge-invariant and IR finite, it can be treated as a standalone channel, and thus NLO corrections can be defined and calculated, without consider full NNNLO corrections to $q\bar{q} \to \gamma\gamma$. However, at NLO, only the contribution from massless quarks are known[18, 16]; the contribution from the top quark is still missing. Naively counting electric charge, after including top quark the cross section can be 1.86 times larger. Therefore, including the contribution from top quark is essential for precise prediction.

2. Method

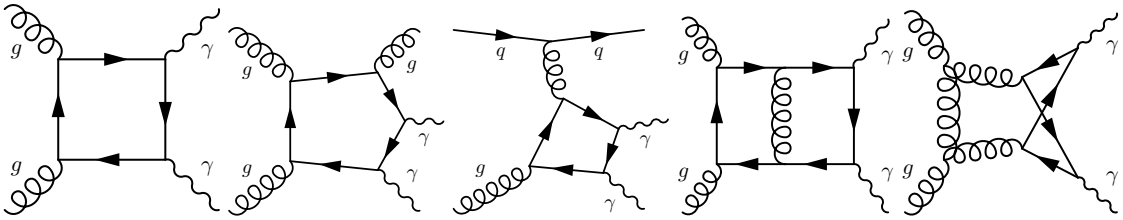

Figure 1: Representative diagrams are shown for the LO, real emission, and virtual contribution.

The cross section for $gg \to \gamma\gamma$ is given by

$$d\sigma^{\mathrm{NLO}} = d\sigma^{\mathrm{LO}} + d\sigma^{R} + d\sigma^{V} + d\sigma^{C} \tag{2.1}$$

where $d\sigma^{\mathrm{LO}}$ is the LO cross section, $d\sigma^{R}$ is the corrections with one more external legs($gg \to \gamma\gamma g, q(\bar{q})g \to \gamma\gamma q(\bar{q}), q\bar{q} \to \gamma\gamma g$), $d\sigma^{V}$ is the corrections with one more loop, and $d\sigma^{C}$ is the counter term from the parton distribution function. We show representative Feynman diagrams in Fig. 1. The last three terms are IR divergent, and only their sum is finite. To handle the IR divergence, we adopt the dipole subtraction method[19], which introduces extra terms for the last three terms so that they become finite, while the extra terms sum up to zero.

PoS(RADCOR2019)024

With the subtraction method available, we also need to calculate the matrix elements. For the real corrections, since they are one-loop process, automated tools are available to compute them. In particular, we adopt MADGRAPH5_AMC@NLO[20] and Recola2[21, 22] to compute those matrix elements.

The main challenge is on the calculation of the two-loop virtual amplitude. In the case that internal lines are massless quarks, the results are known since 2001[23]. However, for massive quark contribution, the results remain unknown. The main reason is that not all master integrals are known analytically; only part of them are known(mostly planar). Instead of analytical approach, we developed a numerical method to calculate them[24].

We use QGRAF[25] to generate corresponding Feynman diagrams, which yields 138 diagrams. We use FORM[26] to deal further proceed the expressions of the amplitude. We adopt projector methods to decompose the amplitudes into form factors. In particular, we work under d-dimension, and we get 10 different tensor bases. We organize the Feynman integrals according to their propagator denominators, obtaining 33 different integral families. After projection, we obtain the form factors written in terms of around 40000 scalar integrals at two-loop. We adopt FIRE5[27] with LiteRed[28, 29] to perform integration-by-parts(IBP) reduction, and we get 1180 master integrals, not counting relations among families. If we consider symmetries among different families, indeed we only have 161 master integrals.

With IBP reductions, it was shown[30, 31] that the derivatives of master integrals can be written in terms of linear combination of themselves, with coefficients are rational expressions on the dimension d and kinematics. Such system of differential equations provide an important way on analytical computation of master integrals. On the other hand, numerical methods for differential equations are well-studied in mathematics. Even if we have multiple kinematics, and thus such system of differential equations is a system partial differential equations by nature, we can integrate all kinematic iteratively. Therefore, numerical algorithms for ordinary differential equations can be applied. We adopt numerical methods for initial value problems to solve the differential equations, which requires numerical value of master integrals in a specific point as the initial condition to fully fix the solution.

We adopt the sector decomposition method[32] to obtain the initial condition. The sector decomposition method is a systematic method that resolving IR and UV divergence for Feynman integrals. After resolving divergences, the remaining integrals can be expanded order-by-order in ε, and numerical integration can be carried out on those integrals. When working in the Euclidean region, saying that the $-i0$ prescription can be discarded, the integrands are well-behaved, and numerical integration is quite efficient with suitable methods. In particular we adopt the quasi-Monte Carlo methods[33]. We implement the sector decomposition method in NIFT[34].

In Table 1, we show numerical results of some relevant Feynman integrals obtain by NIFT and compare it with analytical expression. The corresponding diagrams are shown in Fig. 2. To obtain numerical results to $\mathcal{O}(10^{-7})$ precision, only several seconds are spent.

Since the initial condition is given in the unphysical region, we need to design an integration contour to evolve it to the physical region. The main requirement of the integration contour is that it should not cross branch cuts. It can be also understood that along the integration contour the Feynman integrals can be defined without the $-i0$ prescription, and the integration contour should connect to the target point according to such prescription. For the integrals appear in the two-loop

PoS(RADCOR2019)024

			c_0	time (s)
I_1	IC1	NIFT	$-0.059087788(6)$	1.93
		Analytic	-0.059087788	–
	IC2	NIFT	$-0.056016652(5)$	1.74
		Analytic	-0.056016650	–
I_2^{sub}	IC1	NIFT	0.28729542(1)	3.55
		analytic	0.28729543	–
	IC2	NIFT	0.26181028(1)	3.57
		analytic	0.26181029	–

Table 1: Numerical results for the initial condition obtained with NIFT are shown and compared with analytic results.

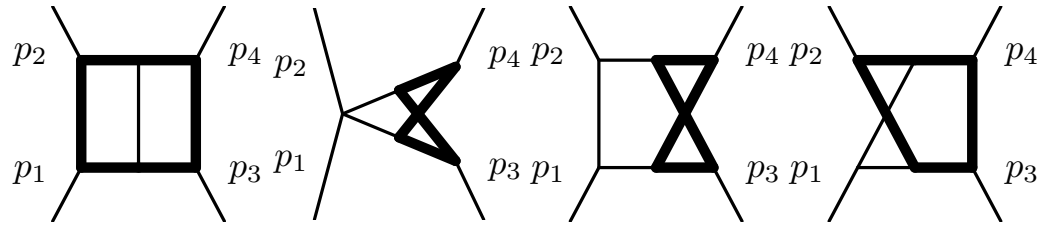

(a) I_1 (b) $I_{2,\text{sub}}$ (c) I_2 (d) I_3

Figure 2: The diagrams of relevant Feynman integrals are shown.

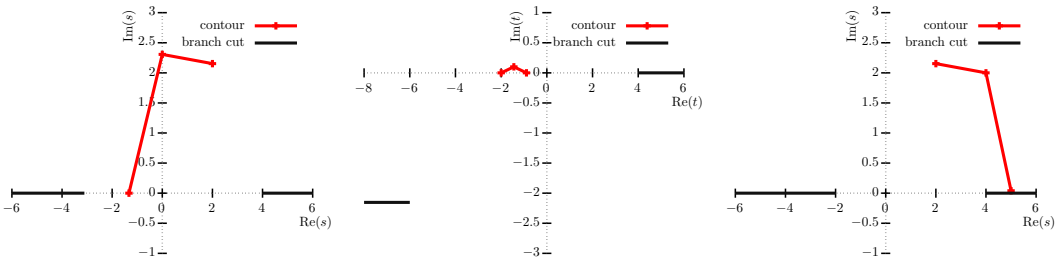

Figure 3: The integration contour and relevant branch cuts are shown.

amplitude of $gg \to \gamma\gamma$, we show the integration contour and branch cuts in Fig. 3.

In Table 2, we compare numerical results obtained via our algorithms with the one from analytical expressions. We can see that $\mathcal{O}(10^{-7})$ precision can be obtained within 1 second. In Table 3, we show results for I_2 and I_3, whose analytical results are unknown. From the discrepancy of results from two differential initial condition, we conclude that our numerical precision is still at $\mathcal{O}(10^{-7})$. For cross check, we also show results obtained from pySecDec, which is much slower and the precision is much lower.

To further speed up the numerical evaluation, we first compute the results at a set of predefined kinematic points in the physical region. After such initial condition table is setup, when evaluating the master integrals at each point, we pick a point in such set and use that result as the initial condition to compute the results. Since the initial condition belongs to the physical region now, it is much closer to the target point, and the integration contour is much simpler and shorter, which

PoS(RADCOR2019)024

$(s=5,t=-2)$		c_0	time (s)
I_1	IC1	$0.573661717 - i0.45602298$	0.11
	IC2	$0.573662051 - i0.45602316$	0.10
	Analytic	$0.573661756 - i0.45602309$	–
I_2^{sub}	IC1	$-0.077764616 + i0.34306744$	0.26
	IC2	$-0.077764595 + i0.34306737$	0.23
	Analytic	$-0.077764620 + i0.34306741$	–

Table 2: Numerical results for I_1 and $I_{2,\text{sub}}$ obtained with our algorithm are shown and compared with analytic results.

$(s=5,t=-2)$		c_0	c_1	c_2	time (s)
I_2	IC1	$0.02188084 - i0.00000002$	$-0.0870259 + i0.05170117$	$-0.246416 - i0.17602070$	0.26
	IC2	$0.02188080 + i0.00000001$	$-0.0870262 + i0.05170118$	$-0.246417 - i0.17602072$	0.23
	pySecDec	$0.02187(3) + i0.00003(3)$	$-0.0869(3) + i0.0518(4)$	$-0.248(2) - i0.175(2)$	$\mathcal{O}(10^4)$
I_3	IC1	$-0.0599222 + i0.4204527$	$-1.2093294 + i1.1271787$	$-3.737851 + i0.435880$	0.74
	IC2	$-0.0599219 + i0.4204528$	$-1.2093298 + i1.1271798$	$-3.737851 + i0.435879$	0.78
	pySecDec	$-0.05998(7) + i0.42048(8)$	$-1.2100(7) + i1.1262(7)$	$-3.737(3) + i0.430(3)$	$\mathcal{O}(10^4)$

Table 3: Numerical results obtained with our algorithm from two different choices of initial conditions for the Feynman integral I_2 and I_3 are shown. The results from pySecDec[35] are also shown for comparison.

yield a significant speedup. Furthermore, since the results of the initial condition table are only need to be computed once, we demand higher accuracy when computing them.

In addition, we observed that t is unchanged during s evolution. Therefore, we reorganize the expressions into a form which is rational expressions on ε and s, with coefficients are polynomials on t. The coefficients are unchanged when evolving the differential equations, and thus they only need to be computed once in each evolution. Similar reorganized can be done for t evolution.

$$\frac{\partial I}{\partial s} = P_s(\{\varepsilon,s,t\};\mathbb{Z})I \to \frac{\partial I}{\partial s} = P_s(\{\varepsilon,s\};\mathscr{R}(\{t\};\mathbb{Z}))I \tag{2.2}$$

$$\frac{\partial I}{\partial t} = P_t(\{\varepsilon,s,t\};\mathbb{Z})I \to \frac{\partial I}{\partial t} = P_t(\{\varepsilon,t\};\mathscr{R}(\{s\};\mathbb{Z}))I \tag{2.3}$$

For better numerical stability in the backward region($|u| \ll |t|, |s|$), we use u to compute the right-hand side of differential equations. That is to say, we adopt the following forms in the backward region.

$$\frac{\partial I}{\partial s} = Q_s(\varepsilon,u;\mathscr{R}(\{t\};\mathbb{Z}))I \tag{2.4}$$

$$\frac{\partial I}{\partial t} = Q_t(\varepsilon,u;\mathscr{R}(\{s\};\mathbb{Z}))I \tag{2.5}$$

In total, 10000 CPU hours are spent to obtain the initial conditions with $\mathcal{O}(10^{-9})$ precision. We expand up to $\mathcal{O}(\varepsilon)$ for 7-propagator master integrals, and $\mathcal{O}(\varepsilon^2)$ for other master integrals. For each phasespace point, it costs around 1 second to evaluate the two-loop amplitude.

PoS(RADCOR2019)024

3. Results

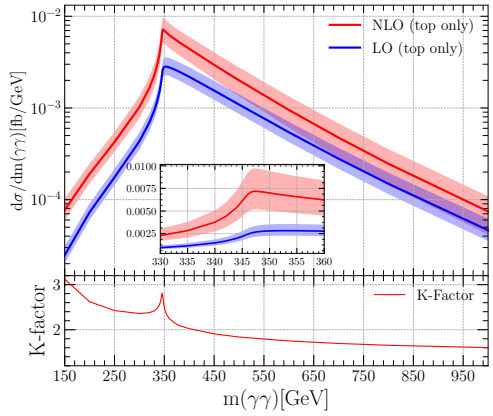

(a) Differential cross section for diphoton production through gluon fusion at the 13TeV LHC, with only top quark contribution

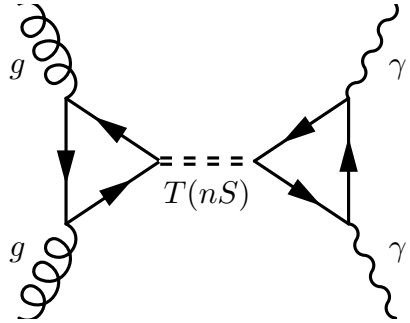

(b) Feynman diagrams for the toponium $T(nS)$ contribution are shown.

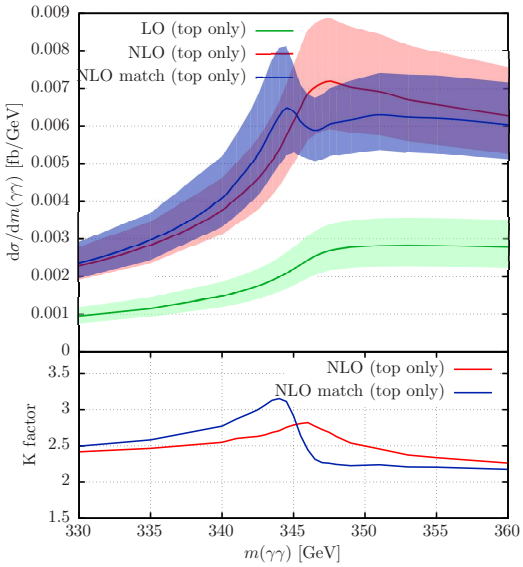

(c) Differential cross section for the top only case are shown at LO, NLO, and NLO matched with resummed results.

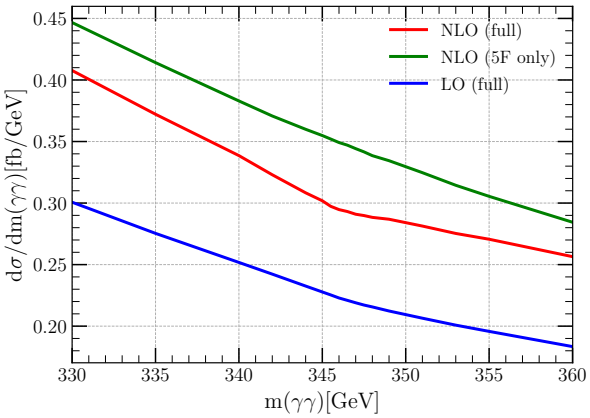

(d) Differential cross section for diphoton production through gluon fusion at the 13TeV LHC in the threshold region are shown for the massless quark only case(5F only), and also including top quark contribution(full).

In Fig. 4a, we show the differential cross section for 13 TeV LHC, only including the top quark contribution. Below top pair threshold, the cross section is strongly suppressed, since the amplitude scaling as $\mathcal{O}(m_t^{-4})$. The differential cross section peaks around top pair threshold, and NLO corrections is large in all regions. In the threshold region, there is a peak in the K-factor, due to the contribution comes from one Coulomb gluon effects exchange.

Indeed, Coulomb gluon exchange yields corrections as α_S/v, which may spoil perturbativity. The contribution from one Coulomb gluon exchange is already included in the two-loop amplitude, and multiple Coulomb gluon exchange is corresponding to the formation of toponium $T(nS)$. The contribution of toponium can be included explicitly by adding the contribution of Feynman

PoS(RADCOR2019)024

diagram(see fig. 4b which corresponding to the following:

$$M^{2L} \to M^{2L,match} = M^{2L} + BG_{DT} \tag{3.1}$$

$$G_{DT} = \sum_{n=1}^{+\infty} -\frac{512m_t^4}{27n^3\pi^5}\alpha_S^3(\arcsin\frac{\sqrt{s}}{2m_t})^4\frac{1}{s-m_n^2} \tag{3.2}$$

and $B = 4\frac{e^2g_s^2}{16\pi^2}Q_t^2\frac{4\pi^2}{m_t^2}$ for $++++,----,++--,--++$ helicity configurations, and $B=0$ for other helicity configurations.

In fig. 4c, we show the differential cross section in the threshold region for the top quark only contribution. NLO corrections are quite large in such region. Furthermore, including multiple Coulomb gluon exchanges leads a peak slightly below top pair threshold, which is corresponding to the lightest toponium $T(1S)$. Away from top pair threshold, the matched results reduce to the fixed order result.

In fig. 4d, we show the differential cross section in the threshold region for the light quark only case and after including top quark contribution. Due to negative interference effects, after including top quark the differential cross section gets reduced. In addition, below and above the top pair threshold we can see that the slope is differential, and such effect is more visible at NLO than at LO.

In the low energy region, the contribution from the top quark can be described as an EFT. Taking only the Abelian part for simplicity, which is corresponding to QED case, the EFT Lagrangian is given by:

$$\mathscr{L} = -\frac{1}{4}F^{\mu\nu}F_{\mu\nu} + \frac{\alpha^2Q^4}{m^4}c_1(F^{\mu\nu}F_{\mu\nu})^2 + \frac{\alpha^2Q^4}{m^4}c_2(\frac{1}{4}F^{\mu\nu}\varepsilon_{\mu\nu\rho\lambda}F^{\rho\lambda})^2 \tag{3.3}$$

$$c_i = c_i^{1L} + \frac{\alpha Q^2}{4\pi}c_i^{2L} + \ldots, \quad i = 1,2 \tag{3.4}$$

The Wilson coefficients can be obtained by matching the amplitude in the low-energy limit in the full theory and EFT. However, naively extrapolating the amplitude to the low-energy limit($s=0$) leads to low precision. Alternatively, we calculate the low energy limit based on Cauchy integral formula,

$$f(s=0) = \frac{1}{2\pi i}\oint \mathrm{d}s\frac{f(s)}{s} = \int_0^{2\pi}\mathrm{d}\phi\, f(s=|r|e^{i\phi}) \tag{3.5}$$

which only need the amplitude with non-zero s. In Table 4 we compare the results obtain via the above approach with analytic results[36], and find that our results are agree with the one in literature, with good precision.

In fig. 5, we show the differential cross section for $m(\gamma\gamma) \in [100, 1000]$ GeV. We can see that below top pair threshold, the top quark contribution is negligible. In the threshold region including top quark decreases the cross section, and above threshold region the cross section becomes larger after including top quark contribution. Moreover, the K-factor for the full case is larger than light quark only case. As the invariant mass increases, the ratio between full case and light quark only case slowly approaching naive six-flavour limit(1.86).

PoS(RADCOR2019)024

	analytic	ours
c_1^{1L}	$\frac{1}{90} = 0.0111111111111\cdots$	0.011111111114(6)
c_2^{1L}	$\frac{7}{90} = 0.0777777777777\cdots$	0.07777777778(1)
c_1^{2L}	$\frac{16}{81} = 0.197530864\cdots$	0.1975308(1)
c_2^{2L}	$\frac{263}{162} = 1.623456790\cdots$	1.6234568(2)

Table 4: Comparison of Wilson coefficients obtained with our approach and analytic results.

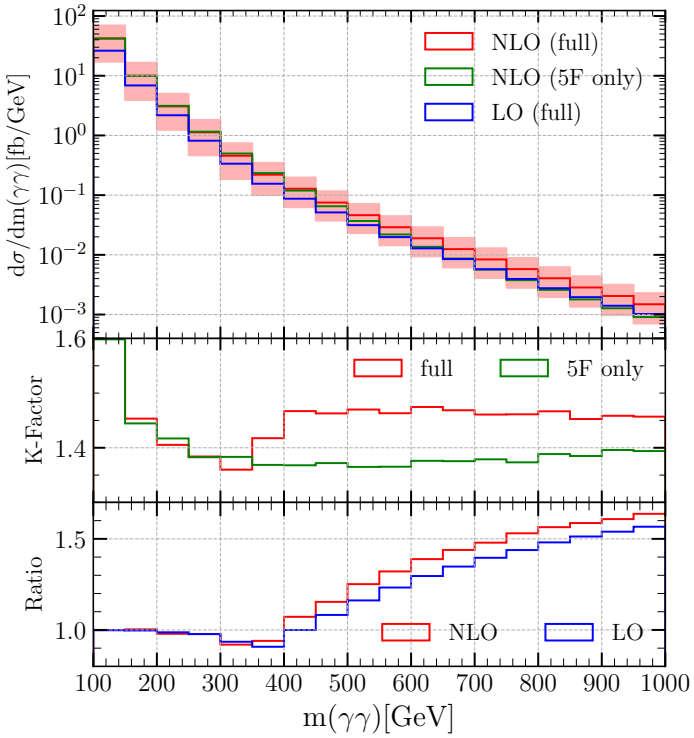

Figure 5: Differential cross section for diphoton production through gluon fusion at the 13TeV LHC are shown.

4. Conclusion

We consider NLO corrections to $gg \to \gamma\gamma$. We include both light quark contributions and the top quark contribution. We developed numerical methods for the two-loop massive amplitudes. We find the NLO corrections are large for the top quark contribution. We also consider resume Coulomb gluon effects in the threshold region and match it with fixed order results. We further examine the low-energy behavior and match it with EFT operators. We find that the slope change below and above the top pair threshold is more visible at NLO than at LO. Going above the top pair threshold, the differential cross section get further enhanced after including the top quark contribution, and more closer to the naive six flavour case at NLO than at LO.

References

[1] CDF collaboration, T. Aaltonen et al., *Measurement of the Cross Section for Prompt Isolated*

PoS(RADCOR2019)024

Diphoton Production Using the Full CDF Run II Data Sample, *Phys. Rev. Lett.* **110** (2013) 101801, [1212.4204].

[2] D0 collaboration, V. M. Abazov et al., *Measurement of the differential cross sections for isolated direct photon pair production in $p\bar{p}$ collisions at $\sqrt{s} = 1.96$ TeV*, *Phys. Lett.* **B725** (2013) 6–14, [1301.4536].

[3] CMS collaboration, S. Chatrchyan et al., *Measurement of the Production Cross Section for Pairs of Isolated Photons in pp collisions at $\sqrt{s} = 7$ TeV*, *JHEP* **01** (2012) 133, [1110.6461].

[4] ATLAS collaboration, G. Aad et al., *Measurement of isolated-photon pair production in pp collisions at $\sqrt{s} = 7$ TeV with the ATLAS detector*, *JHEP* **01** (2013) 086, [1211.1913].

[5] ATLAS collaboration, G. Aad et al., *Observation of a new particle in the search for the Standard Model Higgs boson with the ATLAS detector at the LHC*, *Phys. Lett.* **B716** (2012) 1–29, [1207.7214].

[6] CMS collaboration, S. Chatrchyan et al., *Observation of a new boson at a mass of 125 GeV with the CMS experiment at the LHC*, *Phys. Lett.* **B716** (2012) 30–61, [1207.7235].

[7] CMS collaboration, V. Khachatryan et al., *Search for high-mass diphoton resonances in protonâĂŞproton collisions at 13 TeV and combination with 8 TeV search*, *Phys. Lett.* **B767** (2017) 147–170, [1609.02507].

[8] ATLAS collaboration, M. Aaboud et al., *Search for new phenomena in high-mass diphoton final states using 37 fb^{-1} of proton–proton collisions collected at $\sqrt{s} = 13$ TeV with the ATLAS detector*, *Phys. Lett.* **B775** (2017) 105–125, [1707.04147].

[9] I. Antoniadis, A. Arvanitaki, S. Dimopoulos and A. Giveon, *Phenomenology of TeV Little String Theory from Holography*, *Phys. Rev. Lett.* **108** (2012) 081602, [1102.4043].

[10] M. Baryakhtar, *Graviton Phenomenology of Linear Dilaton Geometries*, *Phys. Rev.* **D85** (2012) 125019, [1202.6674].

[11] P. Cox and T. Gherghetta, *Radion Dynamics and Phenomenology in the Linear Dilaton Model*, *JHEP* **05** (2012) 149, [1203.5870].

[12] G. F. Giudice, Y. Kats, M. McCullough, R. Torre and A. Urbano, *Clockwork/linear dilaton: structure and phenomenology*, *JHEP* **06** (2018) 009, [1711.08437].

[13] D. Chway, R. DermÃ■Åąek, T. H. Jung and H. D. Kim, *Gluons to Diphotons via New Particles with Half the Signal Invariant Mass*, *Phys. Rev. Lett.* **117** (2016) 061801, [1512.08221].

[14] T. Binoth, J. P. Guillet, E. Pilon and M. Werlen, *A Full next-to-leading order study of direct photon pair production in hadronic collisions*, *Eur. Phys. J.* **C16** (2000) 311–330, [hep-ph/9911340].

[15] S. Catani, L. Cieri, D. de Florian, G. Ferrera and M. Grazzini, *Diphoton production at hadron colliders: a fully-differential QCD calculation at NNLO*, *Phys. Rev. Lett.* **108** (2012) 072001, [1110.2375].

[16] J. M. Campbell, R. K. Ellis, Y. Li and C. Williams, *Predictions for diphoton production at the LHC through NNLO in QCD*, *JHEP* **07** (2016) 148, [1603.02663].

[17] M. Grazzini, S. Kallweit and M. Wiesemann, *Fully differential NNLO computations with MATRIX*, *Eur. Phys. J.* **C78** (2018) 537, [1711.06631].

[18] Z. Bern, L. J. Dixon and C. Schmidt, *Isolating a light Higgs boson from the diphoton background at the CERN LHC*, *Phys. Rev.* **D66** (2002) 074018, [hep-ph/0206194].

PoS(RADCOR2019)024

[19] S. Catani and M. H. Seymour, *A General algorithm for calculating jet cross-sections in NLO QCD*, *Nucl. Phys.* **B485** (1997) 291–419, [hep-ph/9605323].

[20] J. Alwall, R. Frederix, S. Frixione, V. Hirschi, F. Maltoni, O. Mattelaer et al., *The automated computation of tree-level and next-to-leading order differential cross sections, and their matching to parton shower simulations*, *JHEP* **07** (2014) 079, [1405.0301].

[21] S. Actis, A. Denner, L. Hofer, A. Scharf and S. Uccirati, *Recursive generation of one-loop amplitudes in the Standard Model*, *JHEP* **04** (2013) 037, [1211.6316].

[22] A. Denner, J.-N. Lang and S. Uccirati, *Recola2: REcursive Computation of One-Loop Amplitudes 2*, *Comput. Phys. Commun.* **224** (2018) 346–361, [1711.07388].

[23] Z. Bern, A. De Freitas and L. J. Dixon, *Two loop amplitudes for gluon fusion into two photons*, *JHEP* **09** (2001) 037, [hep-ph/0109078].

[24] M. K. Mandal and X. Zhao, *Evaluating multi-loop Feynman integrals numerically through differential equations*, 1812.03060.

[25] P. Nogueira, *Automatic Feynman graph generation*, *J. Comput. Phys.* **105** (1993) 279–289.

[26] J. Kuipers, T. Ueda, J. A. M. Vermaseren and J. Vollinga, *FORM version 4.0*, *Comput. Phys. Commun.* **184** (2013) 1453–1467, [1203.6543].

[27] A. V. Smirnov, *FIRE5: a C++ implementation of Feynman Integral REduction*, *Comput. Phys. Commun.* **189** (2015) 182–191, [1408.2372].

[28] R. N. Lee, *Presenting LiteRed: a tool for the Loop InTEgrals REDuction*, 1212.2685.

[29] R. N. Lee, *LiteRed 1.4: a powerful tool for reduction of multiloop integrals*, *J. Phys. Conf. Ser.* **523** (2014) 012059, [1310.1145].

[30] A. V. Kotikov, *Differential equations method: New technique for massive Feynman diagrams calculation*, *Phys. Lett.* **B254** (1991) 158–164.

[31] E. Remiddi, *Differential equations for Feynman graph amplitudes*, *Nuovo Cim.* **A110** (1997) 1435–1452, [hep-th/9711188].

[32] T. Binoth and G. Heinrich, *An automatized algorithm to compute infrared divergent multiloop integrals*, *Nucl. Phys.* **B585** (2000) 741–759, [hep-ph/0004013].

[33] Z. Li, J. Wang, Q.-S. Yan and X. Zhao, *Efficient numerical evaluation of Feynman integrals*, *Chin. Phys.* **C40** (2016) 033103, [1508.02512].

[34] X. Zhao, *In preparation*, .

[35] S. Borowka, G. Heinrich, S. Jahn, S. P. Jones, M. Kerner, J. Schlenk et al., *pySecDec: a toolbox for the numerical evaluation of multi-scale integrals*, *Comput. Phys. Commun.* **222** (2018) 313–326, [1703.09692].

[36] H. Gies and F. Karbstein, *An Addendum to the Heisenberg-Euler effective action beyond one loop*, *JHEP* **03** (2017) 108, [1612.07251].

PoS(RADCOR2019)024